High-power $MoTe_2$-based passively *Q*-switched erbium-doped fiber laser

Mengli Liu (刘孟丽)[1], Wenjun Liu (刘文军)[1,2,*], Peiguang Yan (闫培光)[3], Shaobo Fang (方少波)[2], Hao Teng (滕 浩)[2], and Zhiyi Wei (魏志义)[2]

[1]*State Key Laboratory of Information Photonics and Optical Communications, School of Science, Beijing University of Posts and Telecommunications, Beijing 100876, China*

[2]*Beijing National Laboratory for Condensed Matter Physics, Institute of Physics, Chinese Academy of Sciences, Beijing 100190, China*

[3]*Shenzhen Key Laboratory of Laser Engineering, College of Optoelectronic Engineering, Shenzhen University, Shenzhen 518060, China*

**Corresponding author: jungliu@bupt.edu.cn*

Received October 30, 2017; accepted December 22, 2017; posted online January 26, 2018

Materials in the transition metal dichalcogenide family, including WS_2, MoS_2, WSe_2, and $MoSe_2$, etc., have captured a substantial amount of attention due to their remarkable nonlinearities and optoelectronic properties. Compared with WS_2 and MoS_2, the monolayered $MoTe_2$ owns a smaller direct bandgap of 1.1 eV. It is beneficial for the applications in broadband absorption. In this letter, using the magnetron sputtering technique, $MoTe_2$ is deposited on the surface of the tapered fiber to be assembled into the saturable absorber. We first implement the $MoTe_2$-based *Q*-switched fiber laser operating at the wavelength of 1559 nm. The minimum pulse duration and signal-to-noise ratio are 677 ns and 63 dB, respectively. Moreover, the output power of 25 mW is impressive compared with previous work. We believe that $MoTe_2$ is a promising 2D material for ultrafast photonic devices in the high-power *Q*-switched fiber lasers.

OCIS codes: 160.4330, 140.3540, 140.3510.
doi: 10.3788/COL201816.020007.

Q-switched fiber lasers have been extensively applied in optical telecommunications, environmental sensing, and industrial processing due to their characteristics of narrow pulse duration and high peak power[1–4]. Employing saturable absorbers (SAs) as optical modulator devices is a preferred implementation method for the passively *Q*-switched system because the quality factor *Q* of the optical resonance can be expediently regulated by the intensity-dependent nonlinearity of SAs. At present, semiconductor saturable absorber mirrors (SESAMs) are the mature SAs in commercial applications due to the precise control of the absorption wavelength, saturation threshold, modulation depth, and relaxation time[5]. However, limited bandwidth and high cost become the problems to be solved, which partly restricts the further development of SESAMs[6]. Graphene, as one of representative two-dimensional (2D) nanomaterials, shows extraordinary talents in fiber lasers because of its ultrafast recovery time, high damage threshold, and broadband absorption properties[7–9]. Inspired by graphene, the topological insulators are also found to be excellent saturated absorption materials[10,11]. They have a great advantage in the regulation of light due to their large modulation depth. Black phosphorus has a direct bandgap from 0.3 eV (body structure) to 1.5 eV (single layer)[12,13]. The direct bandgap structure can guarantee ultrafast electronic relaxation, and it is especially beneficial to the field of ultrafast photonics and high-frequency optoelectronics[14]. Gold nanorods have the advantages of high nonlinear coefficient, good optical fiber compatibility, ultrashort response time, and easy preparation. Therefore, the SAs based on gold nanomaterials have also attracted much attention[15].

Meanwhile, investigations on transition metal dichalcogenides (TMDs) are emerging at a fast pace because of their preeminent nonlinear effects and physical properties[16–20]. In TMDs, the atoms in-plane are covalently bonded, while the atoms between each layer are connected by weak van der Waal forces, which is beneficial to the exfoliation of few-layer nanosheets[21]. In the past few years, WS_2 has been employed for the generation of ultrashort optical pulses and exhibited large second-order nonlinear susceptibility[22–25]. MoS_2, as the analogue of WS_2, is also proved to have saturable absorption properties. Moreover, MoS_2-based *Q*-switched and mode-locked fiber lasers have been implemented at 1, 1.5, and 2 μm. Those properties indicate that WS_2 and MoS_2 can be both used as broadband SAs[26–29]. The further explorations of WSe_2 and $MoSe_2$ are also gradually strengthened and developed[30]. The substantial researches on the members of the TMD family indicate that they all exhibit broadband absorption properties and have a great potential in electrooptic applications, which paves the way for the exploration of new members of the TMD family.

Recently, the preparations and electrooptic properties of $MoTe_2$ have been reported[31–34], but the applications in *Q*-switched fiber lasers have hardly been realized. The layer-dependent bandgap is the typical feature of

TMDs. When the $MoTe_2$ is changed from bulk to a single layer, the band structure is transformed from an indirect bandgap into a direct bandgap. Theoretically, the bandgap and saturable absorption bandwidth are inversely proportional. The direct bandgaps of monolayered WS_2, MoS_2, WSe_2, and $MoSe_2$ are 2.1, 1.8, 1.65, and 1.57 eV[35], and the bandgap of monolayer $MoTe_2$ is 1.1 eV, which means the $MoTe_2$ is more likely to be a broadband SA in the TMD family[36,37]. This bandgap is suitable for applying in the near-infrared band. Moreover, compared with MoS_2 and WS_2, $MoTe_2$ has a higher conductivity, which may help to accelerate the relaxation process[38].

Here, we implemented the $MoTe_2$-based Q-switched erbium-doped fiber laser for the first time. The magnetron sputtering process is adopted to deposit layered $MoTe_2$ material on a tapered fiber. The evanescent field appearing at the tapered region of the fused single-mode fiber plays a great role in the interactions with $MoTe_2$. This type of reaction depresses the intensity of the light in the $MoTe_2$ and avoids the damage to the material. When the pump power is regulated to the maximum value (630 mW), the shortest pulse duration and pulse energy of generated Q-switching pulses are 677 ns and 109 nJ, respectively. The corresponding average output power is 25 mW. The experimental results here indicate that the layered $MoTe_2$ is a potential optical modulator device for realizing high-power laser pulses in the nanosecond regime.

Generally speaking, the incorporation schemes of SAs are divided into the following categories: reflection type, embedded system, and side-polished/tapered fiber. The interaction length of the two former ones is short. Moreover, the lights penetrate the material directly in the former two types. Therefore, we consider that the tapered fiber is a proper scheme for our experiment. The fused taper fiber with a 9 mm stretched area and a 15 μm diameter is adopted in the preparation process. The utilization of the evanescent field of the tapered fiber prevents the $MoTe_2$ SA from thermal damage.

With the help of the magnetron sputtering technique, $MoTe_2$ is successfully deposited on the surface of the tapered fiber. In detail, the fused taper fiber and $MoTe_2$ target are placed in a vacuum chamber, the pressure of which is reduced to 3×10^{-3} Pa by a molecular pump. After the bombardment of argon ions, $MoTe_2$ molecules dissociate from the surface of the target, and then deposit on the surface of the tapered fiber. With the advantages of good uniformity, high compactness, strong interfacial adhesion, and low cost, the magnetron sputtering technique is advantageous for massive manufacturing. To get the films with different thicknesses, the sputtering time is the main parameter of regulation. The sputtering time of preparation is 2 min. A scanning electron microscope (SEM) is used to observe the thickness and distribution of the material. As shown in Fig. 1(a), the thickness of $MoTe_2$ is 21 nm. From the inseparable arrangement of the $MoTe_2$ molecules in Fig. 1(b), we can see that its compactness is relatively satisfactory.

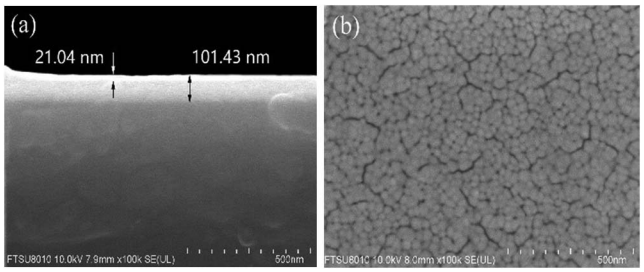

Fig. 1. SEM pictures. (a) Side elevation of the tapered fiber deposited by $MoTe_2$. (b) The magnified morphology of materials on the optical fiber surface.

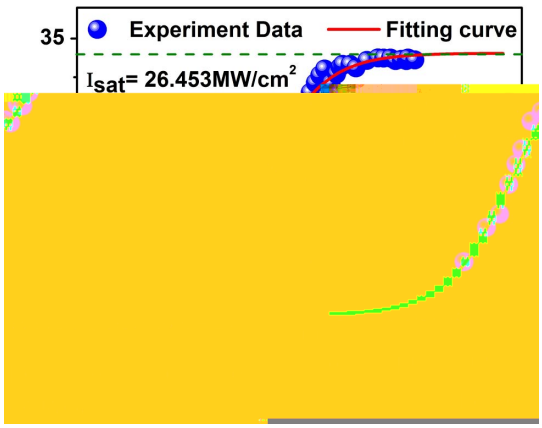

Fig. 2. Saturable absorption characteristics of the $MoTe_2$ SA.

We also characterized the saturable absorption properties of the material by the balanced twin-detector method. The laser source applied in measurement operates at 1550 nm. The shortest pulse duration and repetition rate are 185 fs and 73 MHz, respectively. The principle of this method is to divide the light from the pump source into two parts with the same intensity. Half of the light passes through the SA, and the other half is measured directly. The ratio of the two can reflect the modulation depth of $MoTe_2$ SA. The fitted modulation depth, saturable intensity, and nonsaturable loss are 17.47%, 26.453 MW/cm^2, and 65.95%, respectively, as shown in Fig. 2.

To observe the performance of the prepared $MoTe_2$ SA, a typical ring resonator is constructed as shown in Fig. 3. The central wavelength and maximum output power of the adopted pump are 976 nm and 630 mW, respectively. By pumping through a 980/1550 nm wavelength division multiplexer (WDM), the light excites the energy level transitions in 40 cm long erbium-doped fiber (EDF) (Liekki 110–4/125) to achieve the amplification of optical pulses. 20% of the magnified light is exported through a two-exit optical coupler (OC) to realize the real-time detection of pulses. To get the optimal performance of pulses and balance the polarization state in the cavity, the polarization controller (PC) is employed after OC. Owing to the filtering capabilities of the isolator (ISO), the light in the cavity propagates only in a specific direction. The $MoTe_2$ SA is the main nonlinear device in the laser that

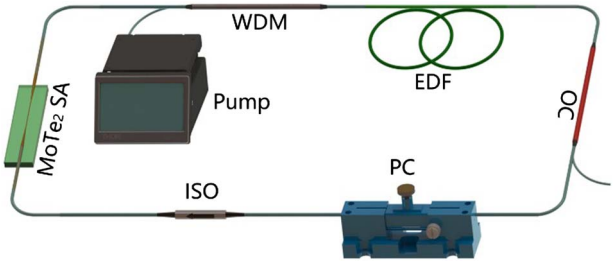

Fig. 3. The experimental arrangement of the $MoTe_2$-based passively Q-switched erbium-doped fiber laser, which includes pump, wavelength division multiplexer (WDM), erbium-doped fiber (EDF), optical coupler (OC), polarization controller (PC), isolator (ISO), and molybdenum ditelluride saturable absorber ($MoTe_2$ SA).

compresses the pulse energy into a narrower time range. The pulse train is constantly detected by a 500 M digital phosphor oscilloscope (Tektronix DPO 3054). The optical spectrum analyzer (Yokogawa AQ6370 C) is used to observe the wavelength of the laser. To check the stability of the whole system, a radio frequency (RF) spectrum analyzer is used to measure the signal-to-noise ratio (SNR) of the pulse.

The self-starting threshold of Q-switched operation is 225 mW. With the increase of the pumping intensity, the laser always maintains a stable operation, as presented in Fig. 4(a). The uniform intensity and smooth waveform of the pulse strings indicate that the $MoTe_2$ has a certain ability to restrain noise. In Fig. 4(b), the pulse has the shortest pulse duration of 677 ns, with an almost symmetric Gaussian distribution. We believe that the pulse duration can be further narrowed under a higher power intensity. According to the inherent characteristics of the Q-switched system, the pulse duration is related to the power intensity. As we know, it is well grounded to reflect the stability of the laser by the intensity of the SNR. The RF spectra of two ranges are both measured in Fig. 4(c). The downward trend in the RF spectra over a wide range indicates the generation of fundamental and harmonic frequencies. Obviously, there are no frequency components of interference. At a narrower span of 500 kHz and a smaller resolution bandwidth (RBW) of 10 Hz, the SNR is measured over 63 dB, which confirms that the Q-switched operation is relatively stable. From Fig. 4(d), we can see that the operating wavelength of the laser is 1559 nm and the spectral width is 0.19 nm.

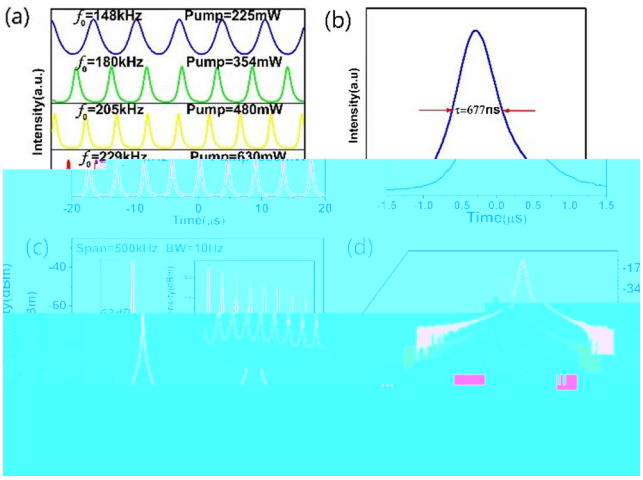

Fig. 4. (a) Pulse distribution. (b) Single pulse duration. (c) RF spectra at two ranges. (d) Spectra at different power levels.

The power-dependent pulse duration and repetition rate are the typical inherent features of the Q-switched system. Therefore, we get the frequency tuning range and the variation of the pulse duration of the laser by regulating the pump intensity. As presented in Fig. 5(a), when the pump power increases from 225 mW to 630 mW, the repetition rate increases tremendously from 148 kHz to 228 kHz. It is worth mentioning that the growth is homogeneous. This is beneficial to the control of the repetition rate of the laser. Although the variation of the pulse duration is not strictly linear, the overall trend is decreasing. The different rates of decline in the low-power region and high-power region reveal the saturable absorption of the $MoTe_2$ SA. The SA at high power is almost at the saturation state and responds insensitively to the change of the power. Change of the power and energy of the optical pulses coincides with the trend of pump power. From Fig. 5(b), the maximum power and energy of the optical pulses are 25 mW and 109 nJ, respectively. The damage threshold of the $MoTe_2$ SA is about 61.7 mJ/cm^2.

In the experiment, we realized the Q-switched pulse output based on the $MoTe_2$ at the wavelength of 1559 nm. This kind of near-infrared band is widely applied in optical communication. In Table 1, we compared the performances of different SA-based Q-switched fiber lasers implemented near 1550 nm. Compared with the Q-switched fiber laser based on other SAs, we find that the Q-switched fiber laser based on the $MoTe_2$ SA has a prominent performance in terms of high output power. We believe that higher output power may be obtained if the cavity loss is further reduced and the pump power is increased. Moreover, due to the smaller bandgap of $MoTe_2$, it will maintain the saturable absorption characteristics of light in a wider bandwidth range.

In this letter, we have achieved the $MoTe_2$-based Q-switched fiber laser for the first time. The method for manufacturing the $MoTe_2$ SA with fused taper type is magnetron sputtering technology. The experimental

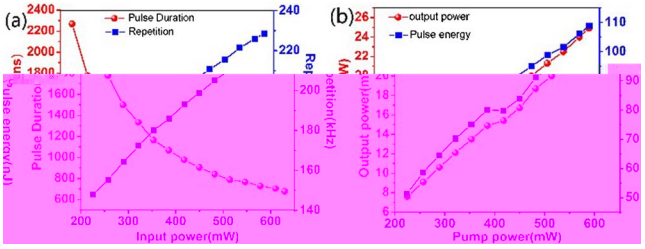

Fig. 5. (a) The pulse duration and repetition rate. (b) The trend curves of output power and pulse energy.

Table 1. Performance Comparison of Passively *Q*-switched EDF Based on Different SAs

Meterials	MoS_2	WS_2	WSe_2	$MoSe_2$	Bi_2Se_3	BP	$MoTe_2$
Wavelength (nm)	1551	1560	1560	1562	1565	1562	1559
Modulation depth	2%	4.48%	3.02%	–	4.3%	10.6%	17.47%
Repetition rate (kHz)	8.77–43.47	91–318	46.3–85.4	16.9–32.8	495–940	7.86–34.32	148–228
Output power (mW)	5.91	17.3	3.16	1.9	22.35	6.67	25
Pulse duration (μs)	3.3	0.16	4.1–9.2	30.4	1.9–7.79	2.96	0.677
Energy (nJ)	160	54.4	484.8	57.9	23.8	194	109
SNR (dB)	50	40	41.9	–	50	53.2	63
References	[39]	[40]	[41]	[42]	[43]	[44]	Our work

results show that the shorter pulse duration and SNR are 677 ns and 63 dB, and the tuning range of the repetition rate is 148 to 228 kHz. It is worth mentioning that the output power of the pulse is 25 mW. The results prepare ultrafast photonic devices for fiber lasers with $MoTe_2$.

This work was supported by the National Natural Science Foundation of China (Grant Nos. 11674036, 11078022, and 61378040), the Beijing Youth Top-notch Talent Support Program (Grant No. 2017000026833ZK08), and the Fund of State Key Laboratory of Information Photonics and Optical Communications (Beijing University of Posts and Telecommunications, Grant Nos. IPOC2016ZT04 and IPOC2017ZZ05).

References

1. R. Paschotta, R. Haring, E. Gini, H. Melchior, U. Keller, H. L. Offerhaus, and D. J. Richardson, Opt. Lett. **24**, 388 (1999).
2. O. Schmidt, J. Rothhardt, F. Roeser, S. Linke, T. Schreiber, K. Rademaker, J. Limpert, S. Ermeneux, P. Yvernault, F. Salin, and A. Tuennermann, Opt. Lett. **32**, 1551 (2007).
3. W. Liu, C. Yang, M. Liu, W. Yu, Y. Zhang, and M. Lei, Phys. Rev. E **96**, 042201 (2017).
4. Z. Sun, A. Martinez, and F. Wang, Nat. Photon. **10**, 227 (2016).
5. T. Hakulinen and O. G. Okhotnikov, Opt. Lett. **32**, 2677 (2007).
6. O. Okhotnikov, A. Grudinin, and M. Pessa, New J. Phys. **6**, 177 (2004).
7. Q. Bao, H. Zhang, Y. Wang, Z. Ni, Y. Yan, Z. Shen, K. Loh, and D. Tang, Adv. Funct. Mater. **19**, 3077 (2009).
8. H. Zhang, Q. Bao, D. Tang, L. Zhao, and K. Loh, Appl. Phys. Lett. **95**, 141103 (2009).
9. Q. Bao and K. Loh, ACS Nano **6**, 3677 (2012).
10. W. Liu, L. Pang, H. Han, W. Tian, H. Chen, M. Lei, P. Yan, and Z. Wei, Sci. Rep. **6**, 19997 (2016).
11. P. Tang, X. Zhang, C. Zhao, Y. Wang, H. Zhang, D. Shen, S. Wen, D. Tang, and D. Fan, IEEE Photon. J. **5**, 1500707 (2013).
12. A. S. Rodin, A. Carvalho, and A. H. C. Neto, Phys. Rev. Lett. **112**, 176801 (2014).
13. C. Han, M. Yao, X. Bai, L. Miao, F. Zhu, D. Guan, S. Wang, C. Gao, C. Liu, D. Qian, Y. Liu, and J. Jia, Phys. Rev. B **90**, 085101 (2014).
14. Y. Chen, G. Jiang, S. Chen, Z. Guo, X. Yu, C. Zhao, H. Zhang, Q. Bao, S. Wen, D. Tang, and D. Fan, Opt. Express **23**, 12823 (2015).
15. X. Wang, N. Zhao, H. Liu, R. Tang, Y. Zhu, J. Xue, Z. Luo, A. Luo, and W. Xu, Chin. Opt. Lett. **13**, 081401 (2015).
16. W. Liu, M. Liu, M. Lei, S. Fang, and Z. Wei, IEEE J. Sel. Top. Quantum Electron. **24**, 1 (2018).
17. A. Geim and I. Grigorieva, Nature **499**, 419 (2013).
18. P. Yan, A. Liu, Y. Chen, H. Chen, S. Ruan, C. Guo, S. Chen, I. Li, H. Yang, J. Hu, and G. Cao, Opt. Mater. Express **5**, 479 (2015).
19. W. Liu, L. Pang, H. Han, Z. Shen, M. Lei, H. Teng, and Z. Wei, Photon. Res. **4**, 111 (2016).
20. H. Chen, Y. Chen, J. Yin, X. Zhang, T. Guo, and P. Yan, Opt. Express **24**, 16287 (2016).
21. F. Koppens, T. Mueller, P. Avouris, A. Ferrari, M. Vitiello, and M. Polini, Nat. Nanotechnol. **9**, 780 (2014).
22. W. Liu, L. Pang, H. Han, K. Bi, M. Lei, and Z. Wei, Nanoscale **9**, 5806 (2017).
23. M. Liu, W. Liu, L. Pang, H. Teng, S. Fang, and Z. Wei, Opt. Commun. **406**, 72 (2018).
24. C. Janisch, Y. Wang, D. Ma, N. Mehta, A. L. Elías, N. Perea-López, M. Terrones, V. Crespi, and Z. Liu, Sci. Rep. **4**, 5530 (2014).
25. W. Liu, L. Pang, H. Han, M. Liu, M. Lei, S. Fang, H. Teng, and Z. Wei, Opt. Express **25**, 2950 (2017).
26. H. Zhang, S. Lu, J. Zheng, J. Du, S. Wen, D. Tang, and K. Loh, Opt. Express **22**, 7249 (2014).
27. K. Wang, J. Wang, J. Fan, M. Lotya, A. Neill, D. Fox, Y. Feng, X. Zhang, B. Jiang, and Q. Zhao, ACS Nano **7**, 9260 (2013).
28. S. Wang, H. Yu, H. Zhang, A. Wang, M. Zhao, Y. Chen, L. Mei, and J. Wang, Adv. Mater. **26**, 3538 (2014).
29. Z. Luo, D. Wu, B. Xu, H. Xu, Z. Cai, J. Peng, J. Weng, S. Xu, C. Zhu, F. Wang, Z. Sun, and H. Zhang, Nanoscale **8**, 1066 (2016).
30. D. Mao, X. She, B. Du, D. Yang, W. Zhang, K. Song, X. Cui, B. Jiang, T. Peng, and J. Zhao, Sci. Rep. **6**, 23583 (2016).
31. D. H. Keum, S. Cho, J. H. Kim, D. Choe, H. Sung, M. Kan, H. Kang, J. Hwang, S. W. Kim, H. Yang, K. J. Chang, and Y. H. Lee, Nat. Phys. **11**, 482 (2015).
32. Y. Ma, Y. Dai, M. Guo, C. Niu, J. Lu, and B. Huang, Phys. Chem. Chem. Phys. **13**, 15546 (2011).
33. L. Zhou, K. Xu, A. Zubair, A. D. Liao, W. Fang, F. Ouyang, Y. H. Lee, K. Ueno, R. Saito, T. Palacios, J. Kong, and M. S. Dresselhaus, J. Am. Chem. Soc. **137**, 11892 (2015).
34. J. Yang, T. Lu, Y. Myint, J. Pei, D. Macdonald, J. Zheng, and Y. Lu, ACS Nano **9**, 6603 (2015).
35. K. Wu, B. Chen, X. Zhang, S. Zhang, C. Guo, C. Li, P. Xiao, J. Wang, L. Zhou, W. Zou, and J. Chen, Opt. Commun. **406**, 214 (2018).
36. C. Ruppert, O. B. Aslan, and T. F. Heinz, Nano Lett. **14**, 6231 (2014).
37. D. Mao, B. Du, D. Yang, S. Zhang, Y. Wang, W. Zhang, X. She, H. Cheng, H. Zeng, and J. Zhao, Small **12**, 1489 (2016).

38. A. Kumar and P. K. Ahluwalia, Eur. Phys. J. B **85**, 186 (2012).
39. Y. Huang, Z. Luo, Y. Li, M. Zhong, B. Xu, K. Che, H. Xu, Z. Cai, J. Peng, and J. Weng, Opt. Express **22**, 25258 (2014).
40. H. Chen, L. Li, S. Ruan, T. Guo, and P. Yan, Opt. Eng. **55**, 081318 (2016).
41. B. Chen, X. Zhang, K. Wu, H. Wang, J. Wang, and J. Chen, Opt. Express **23**, 26723 (2015).
42. H. Ahmad, M. Suthaskumar, Z. C. Tiu, A. Zarei, and S. W. Harun, Opt. Laser Technol. **79**, 20 (2016).
43. Z. Yu, Y. Song, J. Tian, Z. Dou, H. Guoyu, K. Li, H. Li, and X. Zhang, Opt. Express **22**, 11508 (2014).
44. H. Mu, S. Lin, Z. Wang, S. Xiao, P. Li, Y. Chen, H. Zhang, H. Bao, S. P. Lau, and C. Pan, Adv. Opt. Mater. **3**, 1447 (2015).